Spatial Statistics for Micro/Nanoelectronics and Materials Science

E. Miranda, D. Jiménez, J. Suñé,
É. O'Connor, S. Monaghan, K. Cherkaoui, and P.K. Hurley

Abstract – Spatial statistics is a specialized branch of statistics aimed to provide information about the locations of randomly distributed objects in 1, 2 or 3 dimensions. The analysis involves data exploration, parameter estimation, model fitting and hypothesis formulation. In particular, in this work, we present some recent advances in the characterization of the spatial distribution of breakdown spots over the gate electrode of Metal-Insulator-Semiconductor and Metal-Insulator-Metal structures. The spots are regarded as a two-dimensional point pattern, which is analyzed using intensity plots, spatial counting methods, inter-event distance histograms and functional summary estimators. The methods reported here are general so that they can be applied to many different research fields.

I. Introduction

Spatial statistics is a specific branch of statistics aimed to describe and characterize the locations of randomly distributed objects in 1, 2 or 3D [1]. The objects can be trees in a forest, stars in the sky, cells in biological tissue, point-like defects in a silicon crystal wafer, etc., which from the mathematical viewpoint are regarded as a spatial point pattern. If any inherent or attributed property of the objects, such as size, color, type, status, etc., is considered, we have what is called a marked point pattern, and this information *m* can appear as one or more additional coordinates in the point location vector *(x,y,z,m)*. A number of scientific disciplines such as archaeology, biology, astronomy, ecology, medicine, epidemiology and materials science have long made extensive use of the techniques developed to analyze marked point patterns [1,2]. Moreover, thanks to the aid of new technologies for collecting data and the availability of specialized software, the number of applications in other areas such as image analysis and geographical information systems is rapidly increasing. As in other branches of statistics, spatial statistics basically deals with exploratory data analysis, parameter estimation, model fitting and hypothesis formulation. In this work, we will focus the attention exclusively on exploratory data issues, and to this end we will make use of a number of numerical and functional characteristics able to summarize 2D data sets.

E. Miranda, D. Jiménez, and J. Suñé are with the Departament d'Enginyeria Electrònica, Universitat Autònoma de Barcelona, Bellaterra 08193, Spain, E-mail: enrique.miranda@uab.cat.

E. O'Connor, S. Monaghan, K. Cherkaoui, and P.K. Hurley are with the Tyndall National Institute, Cork, Ireland.

The main objectives of spatial statistics are to detect whether or not a point pattern exhibits some kind of interaction among the points, and if possible to determine its origin. The interaction can be reflected in the inter-point distances (repulsion or attraction) or can somehow affect the mark values. Correlation between distances and mark values may also occur, which largely increases the complexity of the problem to be analyzed. A very central issue in spatial statistics is that not only the locations of the points are important but also the size of the observation window since this can seriously affect the conclusions drawn from the statistical analysis. The observation window can be artificial or natural depending on the selected boundaries. As shown in Fig. 1, an improperly chosen observation window can lead us to spuriously conclude that a given point pattern suffers from some kind of aggregation effect. In our case, the observation window always coincides with the device area but in some cases a particular region of the device could require special attention. This is called a "zoomed" approach.

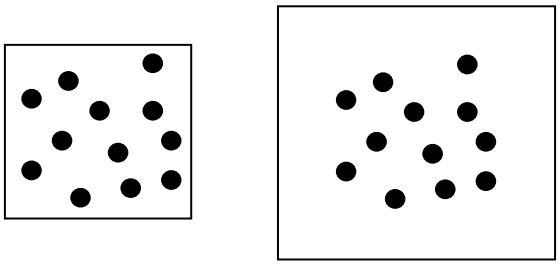

Fig. 1- The same point pattern with two different observation windows

It is worth mentioning that the standard reference model of a point process is the homogeneous Poisson point process with intensity λ, where λ is the expected number of points per unit area. This process is referred to as the Complete Spatial Randomness (*CSR*) process and is commonly regarded as the null hypothesis model in spatial statistics [1,2]. Even though the literature often refers to a point process as a stochastic model for a point pattern, it should be kept in mind that in most cases time-independent problems are assumed (even if it is not the case). As will be shown in this work, exploratory analysis of a spatial point process involves a number of statistical tools such as intensity plots, empirical and theoretical distance histograms and functional summary estimators. These methods will be discussed in Section III.

This paper mainly focuses on the spatial distribution of breakdown (BD) spots over the gate electrode area of Metal-Insulator-Semiconductor (MIS) and Metal-Insulator-Metal (MIM) devices. This represents a good example of point pattern analysis with natural boundaries. Some years ago, Alam *et al* [3] raised the question whether the BD spot locations in MIS devices were spatially correlated or they truly followed a *CSR* model. The issue has major reliability implications since the transistor lifetime is expected to be sensitive to the degree of spatial and temporal correlations among BD spots. Even though the temporal correlation had received extensive attention in the past [4,5], the problem of the 2D spatial distribution was at that time an open subject. To our knowledge, the first study about the BD spots distribution in MIS devices using spatial statistics was reported in [6].

It has been suggested that the interaction among spots may arise because of local variations of the potential distribution in the semiconductor substrate in the vicinity of the leakage sites [4], or by local enhancements of the trap generation rate during the dielectric wearout phase [5]. However, as discussed in [2], even in the absence of actual interactions, some deviation from *CSR* may arise as a consequence of "environmental" variations (in our case oxide thickness, permittivity, extrinsic defects, etc.) leading to local patches with relatively high or low concentrations of events. Of course, as occurs in other branches of statistics, this limits the conclusions which can be drawn, consequently, factors like these should always be taken into account. On the contrary, the observation of *CSR* can help us to rule out such environmental variations.

In principle, in order to assess whether the BD spot locations follow a *CSR* process or not, two approaches are possible: firstly, one can infer the spatial distribution from the first BD event statistics in many devices (this is the standard approach), or alternatively, one can analyze the distribution of a large number of BD spots in a single device. Concerning the first method, the experimental fact that the Weibull slopes β corresponding to different gate areas are independent of the area is well known to be a consequence of the Poisson area scaling [7]. However, this approach often relies on the detection of a single BD event per device, which precludes the possibility of exploring the interaction between spots. Successive breakdown statistics is also consistent with *CSR* but the analysis is again limited in practice to a few events per device [5]. In connection with the second method, in [1], the correlation among spots was evaluated using simulated data compatible with the current distribution in a four-terminal device fabricated to that aim. The results obtained led the authors to conclude that the BD spots do not exhibit spatial correlation and therefore that they are well represented by a *CSR* process. As we can see, *CSR* seems to be the rule for BD spots generation so that it would be of interest to know and to have the analytical tools to check if this is always the case. As will be shown in Section III, this hypothesis may sometimes fail so that it should be considered with caution.

II. Devices and Experimental Details

Two types of samples are analyzed in this work. The first set of devices consists of MgO films with nominal oxide thickness t_{ox}=20 nm deposited by e-beam evaporation on *n*-type Si and *n*-type InP substrates. The MgO/Si and MgO/InP samples were capped in-situ with 100 nm of amorphous silicon (α-Si) using a second e-beam source. For the NiSi gate process, nickel was deposited by e-beam evaporation (~80 nm) through a patterned resist mask followed by a lift-off process. The area of the devices (squares) tested ranges from $9.0\text{x}10^{-6}$ to $1.0\text{x}10^{-4}$ cm^2. The second set of devices discussed here consists of $Pt/HfO_2/Pt$ capacitors formed on a 200 nm-thick thermal SiO_2 grown on *n*-type Si substrates. HfO_2 (10 nm) is grown by atomic layer deposition. Then, lithography and a lift-off process are used to form arrays of circular area MIM devices. Access to the bottom Pt metal is enabled via a dry etching technique using a mask/resist process that removes the HfO_2 to the bottom Pt metal while at the same time protecting the top Pt metal of the patterned devices. This process also protects an oxide region that extends 25 µm beyond the perimeter edge of the top metal, which is supposed to eliminate edge effects on the electrical properties of the devices.

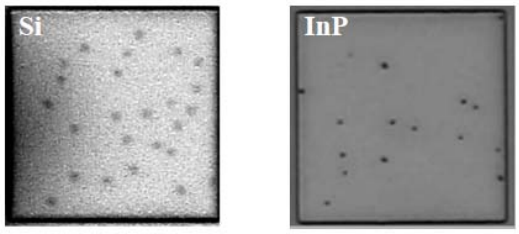

Fig. 2 - BD spots distribution in NiSi/MgO/Si and NiSi/MgO/InP devices.

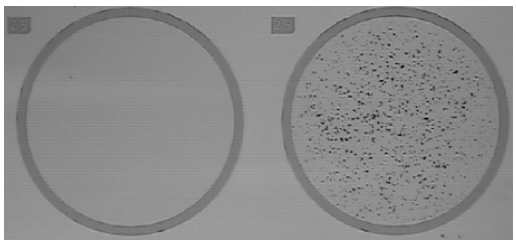

Fig. 3 - $Pt/HfO_2/Pt$ capacitors without and with BD spots.

In order to generate the spots, the devices were subjected to ramped voltage stresses (positive or negative). The thermal effects associated with the oxide BD events

are so important that permanent localized damaged areas can be observed as black dots distributed over the gate electrode area (see Figs. 2 and 3). The spots were photographed using a standard microscope and the images were digitalized for statistical processing. For the sake of simplicity, we will confine our attention to unmarked point patterns, i.e. the size of the BD spots will not be considered here. The statistical analysis is carried out using the Spatstat package for R language [8].

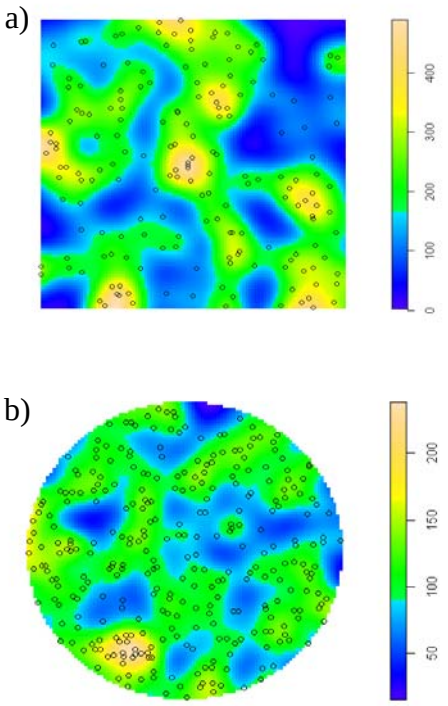

Fig. 4 - Typical intensity plots for a) MIS and b) MIM structures. The scales show the number of points (locally weighted) per unit area.

III. Point Pattern Analysis Methods Applied to BD Spots Characterization

In order to summarize a point pattern structure, numerical and functional characteristics can be used. As for any estimate computed from a set of observations, two interpretations are possible: firstly, estimates are used to make inferences about the process from which the data set was chosen at random (*inferential statistics*) and secondly, estimates can be viewed as descriptive of the particular data set used to compute the estimate (*descriptive statistics*). In spatial statistics, we can adopt either of the two viewpoints. The most important numerical summary characteristic for a point process is the intensity λ, *i.e.* the average density of points. Additional insight on the distribution of the spots can be achieved using the quadrat count method in combination with the Morishita index. Distance methods involve analyzing the distance distribution among all points and comparing to the corresponding theoretical distributions. Concerning the functional summary characteristics, a number of estimators called *F*, *G*, *J*, *K* and *g* have been proposed, which provide complementary statistical information on the point pattern distribution. The central idea of using these functions is that they can be explicitly calculated for a *CSR* process. The resulting expressions are then compared with the empirical curves directly computed from the experimental point locations. These methods are now discussed in detail.

A. Intensity plots

The very basic analysis tool in spatial statistics is the intensity plot. Figure 4 shows typical intensity plots for MIS and MIM devices with different shapes. In both cases the actual dimensions were normalized to unity. The local intensity $\lambda(r)$ is defined as the density of points in an area $A(r)$, where r is some radius. The plots are obtained using an isotropic Gaussian kernel with a bandwidth parameter, which determines the degree of smoothing. Notice that the intensity varies from location to location, but this is consistent with *CSR*, in which the points are not uniformly spread but there are empty gaps and clusters of points.

B. Quadrat counts method (QCM)

In this method, the window containing the point pattern is divided into a grid of rectangular tiles or “quadrats”, and the number of points falling in each quadrat is counted. The quadrats are square by default but may have arbitrary shape as well. One major drawback of QCM is that the choice of the quadrat size is strongly linked to the spatial scale of the problem, which establishes a limit to the applicability of the method. The basic idea behind the QCM test is to find evidence against the null hypothesis of a *CSR* process.

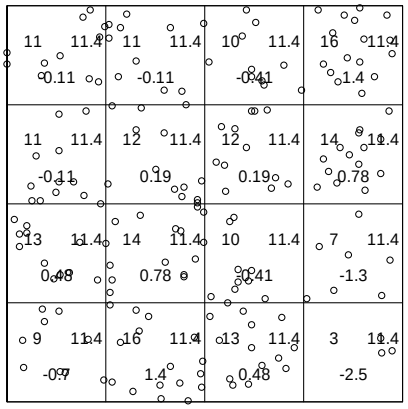

Fig. 5 - QCM plot for the data shown in Fig. 4.a including the observed spots (upper left), the expected number of spots using a Poisson model (upper right) and the Pearson residuals (second row).

As mentioned above, the device area is partitioned into Q quadrats and the number of spots falling in the i-th quadrat $n[i]$ is counted. Assuming that the $n[i]$ are independent and identically-distributed Poisson random variables with the same expected value, the Pearson χ^2 test can be evaluated, which in turn can be used to reject or accept the *CSR* model. In the example illustrated in Fig. 5, the observed data, the expected data and the Pearson residuals (=[(observed)-(expected)]/√expected) are shown. A small Pearson residual indicates good agreement with *CSR*. A major problem with this approach is that the final conclusion may depend on the quadrats number. Fortunately, the question can be overcome by considering the Morishita index *MI*, which is defined as [9]:

$$MI = Q\sum_{i=1}^{Q}\frac{n[i]\left(n[i]-1\right)}{N\left(N-1\right)} \qquad (1)$$

where N is the total number of spots. Figure 6 shows *MI* as a function of the quadrat size. The pattern can be considered completely random when $MI \approx 1$. For our example, $Q \leq 4x4=16$ quadrats are recommended for carrying out the analysis.

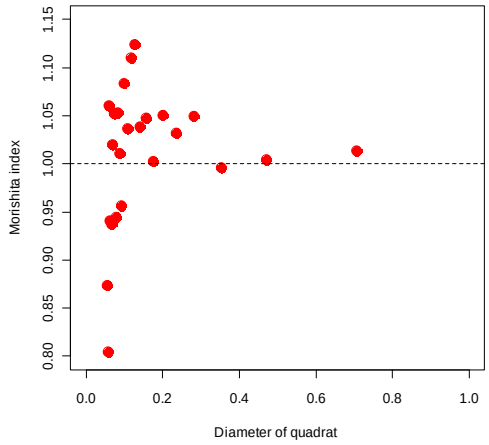

Fig. 6 - Morishita index (1) as a function of the quadrat size.

C. Distance methods

A totally different approach is to examine the distance distribution among all points. Figure 7 shows the empirical distribution (data from Fig. 4.a) as well as the corresponding theoretical probability density (solid line) given by the following expression [10]:

$$f(d) = \begin{cases} 4d\left[\frac{\pi}{2} - 2d + \frac{d^2}{2}\right] & 0 \le d \le 1 \\ 4d\left[\arcsin\left(\frac{1}{d}\right) - \arccos\left(\frac{1}{d}\right) - 1 - \frac{d^2}{2} + 2\sqrt{d^2-1}\right] & 1 < d \le \sqrt{2} \end{cases} \qquad (2)$$

(2) is reached under the hypothesis that the x- and y-coordinates of each data point are uniformly distributed in the range [0,1]. From Fig. 7, it must be noted that the agreement between the histogram and the solid curve is very good, which seems to indicate that the points follow a *CSR* process. However, the main problem with this method is that the details of the tails of the distribution are sometimes lost.

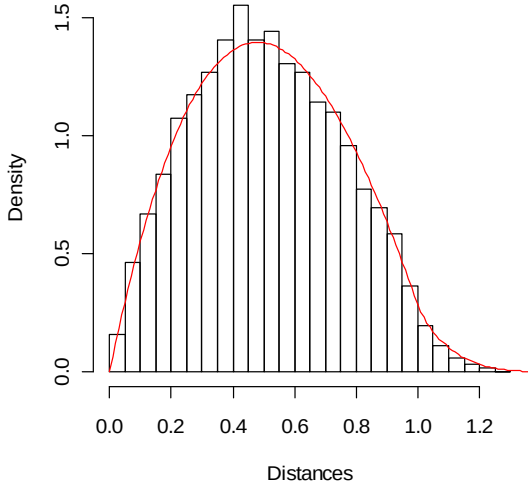

Fig. 7 - Distance histogram for the points shown in Fig. 4.a. The solid lines is calculated using (2).

D. Functional summary characteristics

Several functional summary characteristics have been proposed to characterize a point pattern. These are called F, G, J, K and g and they are defined as follows:

D.1 The *F-test*

The empty space function, the contact distribution or the "point-to-event" distribution F, is the cumulative distribution of the distance from a fixed point in space to the nearest point. F is a useful statistic summarizing the sizes of gaps in the pattern. Another interpretation of F is the probability that a randomly located disc of radius r contains at least one point. For a *CSR* process with intensity λ:

$$F_{CSR}(r) = 1 - \exp(-\lambda\pi r^2) \qquad (3)$$

While $F > F_{CSR}$ suggests that empty space distances are shorter than for a *CSR* process (regularly space pattern), $F < F_{CSR}$ suggests a clustered pattern. In Fig. 8.a. the dashed line is computed using (3) and the solid line is found using the point locations from Fig. 4.a. The same applies for Figs. 8b-8d and expressions (4)-(7).

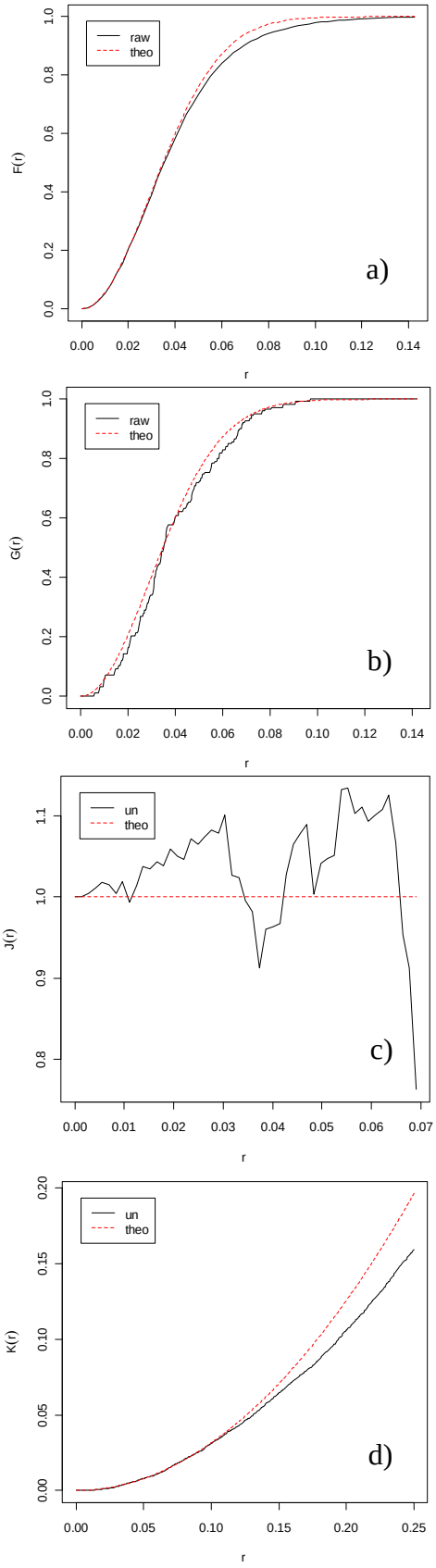

Fig. 8 - Functional summary estimators for the data shown in Fig. 4.a.

*D.2 The **G**-test*

The nearest neighbour distance distribution function or the "event-to-event" distribution G is the cumulative distribution of the distance from a typical random point to the nearest other point. G has the same expression as F for a *CSR* process:

$$G_{CSR}(r) = 1 - \exp(-\lambda\pi r^2) \quad (4)$$

While $G>G_{CSR}$ suggests that nearest neighbour distances are shorter than for a *CSR* process (clustered pattern), $G<G_{CSR}$ suggests a regular pattern. See Fig. 8.b.

*D.3 The **J**-test*

J is the Van Lieshout-Baddeley function and is a measure of the deviations from F and G . J is defined as:

$$J = (1-G)/(1-F) \quad (5)$$

$J_{CSR}=1$ corresponds to a *CSR* process, while $J>1$ suggests regularity and $J<1$ suggests clustering. See Fig. 8.c.

*D.4 The **K**-test*

The Ripley's K function is defined so that $\lambda K(r)$ equals the expected number of random points within a radius r of a typical random point. For a *CSR* process:

$$K_{CSR}(r)=\pi r^2 \quad (6)$$

While $K>K_{CSR}$ suggests clustering, $K<K_{CSR}$ suggests a regular pattern. See Fig. 8.d.

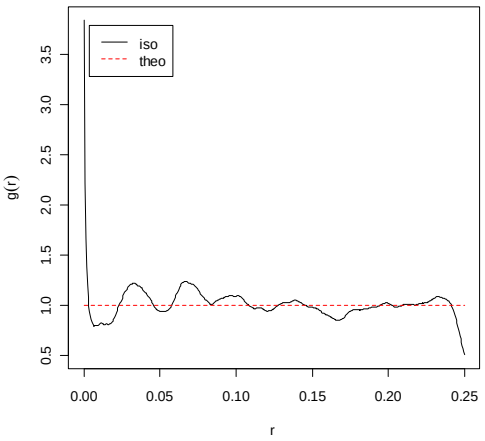

Fig. 9 - Pair correlation function for the data shown in Fig. 4.a.

D.5 The ***g***-test

Perhaps, the most important functional summary statistics available for point patterns is the pair correlation function g. This is also known as the reduced second moment function of the point process and is considered the best estimator for inferential purposes. *g(r)* is the probability of observing a pair of points separated by a distance r divided

by the corresponding probability for a Poisson process and can be found as:

$$g(r) = [dK(r)/dr]/(2\pi r) \quad (7)$$

$g_{CSR}(r)=1$ corresponds to a *CSR* process, $g>1$ suggests clustering or attraction, while $g<1$ suggests inhibition or regularity. The estimator fails for r values close to 0. In practice g is not calculated from (7) but a different numerical approach is used (compare Figs. 8.d and 9). As shown in Fig. 9, $g\approx1$ for the realization under analysis, which indicates that the generation of spots follows a *CSR* process. This is what is expected for an oxide layer with a uniform generation of defects, which in turn is an indicator of the quality of the dielectric film. No particularly weak region is detected.

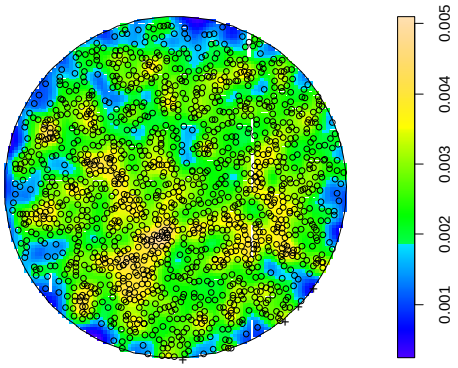

Fig. 10 - Pt/HfO_2/Pt capacitor with a lower density of spots in the periphery.

Interestingly, Fig. 10 shows a case in which the BD spots' spatial distribution clearly departs from *CSR*. Even though a large number of spots were detected, close to the periphery of the device the density of spots is lower than expected. The origin of this deviation is not yet clear and it is not related to the circular shape since rectangular devices exhibit the same deviation. It is possible that the electric field at the edge is lower than in the center of the structure because of some process-related effect. A zoomed analysis, far from the periphery of the device, reveals that the spots follow a *CSR* process. Anomalies in the distribution of BD events in MOS devices were also reported in Refs. [11,12]

IV. Further Applications in the Fields of Nanotechnology and Materials Science

Some of the methods reported above have been widely used in microelectronics (defects metrology in wafers) [13] and materials science (corrosion patterns, random packing, structure factor, coordination shells, etc.) [14-15]. In this Section we just want to highlight the power of the pair correlation function g as a characterization tool for spatial point patterns. Importantly, as mentioned earlier, a complete study on this subject would require the analysis of marked point processes where, for example, the size of the objects under consideration is included the treatment. As will be demonstrated next, occasionally the interpretation of the g plot is not straightforward and requires some expertise. For a complete discussion see [1].

As a first example, Fig. 11.a shows the spatial distribution of Co/Pt nanodots on a SiO_2 substrate. The data was obtained from Prof. Oepen's group webpage [16]. According to the authors, the nanodots are 18 nm-diameter and the picture size is 0.8 μm x 0.8 μm. The circles in Fig. 11.a correspond to the location of the centers of the nanodots. A minimum interpoint distance of 15-20 nm is detected from Fig. 11.b in agreement with the reported spot sizes. 294 points were counted with $\lambda=4.69\text{x}10^{-4}$ points/nm^2 and a mean nearest neighbour distance of 32 nm. It is worth mentioning that in this case there is no real repulsion effect at short scale and that the size of the nanodots (not shown here) establishes a minimum separation distance between the points.

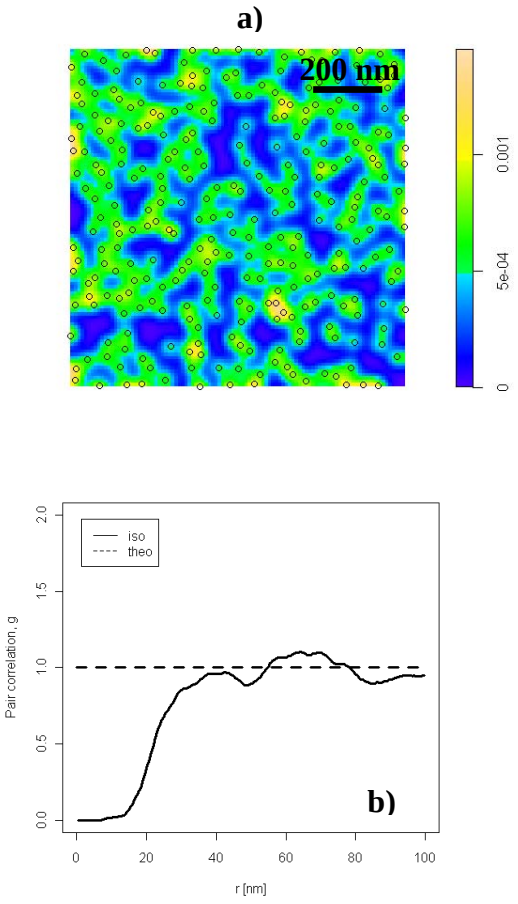

Fig. 11- Distribution of Co/Pt nanodots on a SiO_2 substrate [16], a) intensity plot, b) pair correlation function g.

The second case study corresponds to a SEM image of ferromagnetic dots with domain walls in the nanometer range (see Fig. 12.a). According to the information provided by the authors the average dot size is about 63±6 nm (data taken from Schuller's nanoscience group webpage [17]), which is totally consistent with the $g\approx0$ region in Fig.12.b. This is a highly ordered structure with a range of most frequent short interpoint distances of 94 nm (maximum of g) and a distance from a typical point to regions with a small number of points beyond the nearest neighbours of 135 nm (first minimum of g). Notice from Fig. 12.b the important deviations from *CSR* occurring at these two length scales, which is an indication of the existence of short-range order in the point process. 122 points were counted with $\lambda=1.25\text{x}10^{-4}$ points/nm^2 and a mean nearest neighbour distance of 86 nm.

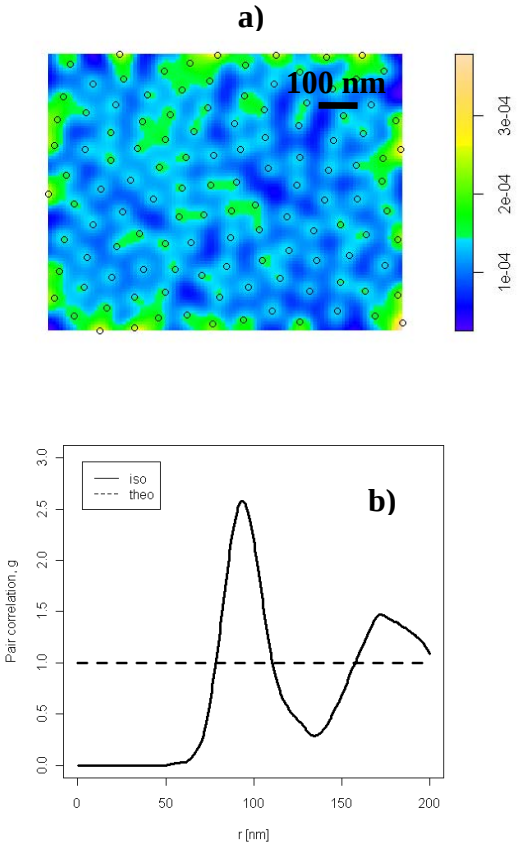

Fig. 12- Distribution of ferromagnetic dots [17], a) intensity plot, b) pair correlation function g.

Finally, the last example (see Fig. 13.a) shows the nucleation of colloidal Pt nanocrystals in solution (data taken from Ref. [18]). This is a typical aggregation process. The first maximum in Fig. 13.b reveals that the most frequent short interpoint distance is around 3 nm. The second maximum at 6 nm corresponds to the most frequent longer inter-point distance (distance from typical point to regions with further neighbours). In this case, 495 points were counted with $\lambda=4.22\text{x}10^{-2}$ points/nm^2 and a mean nearest neighbour distance of 2.74 nm.

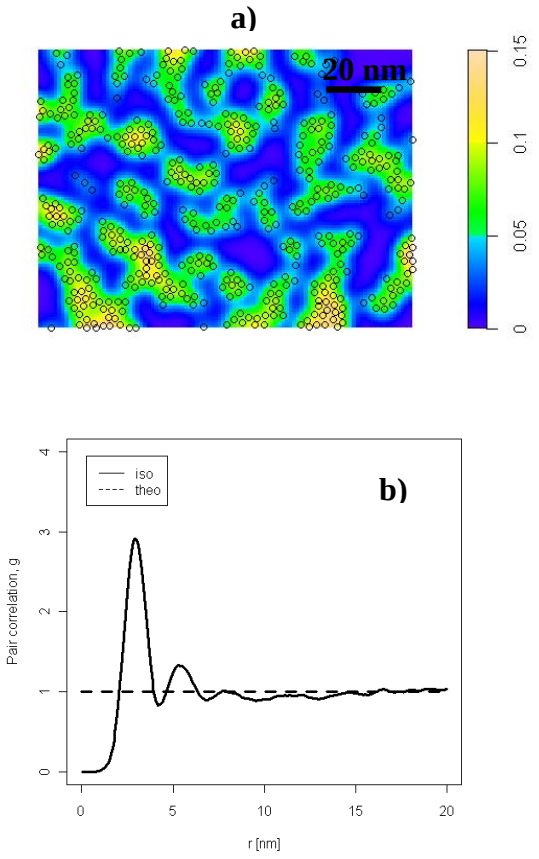

Fig. 13- Distribution of colloidal Pt nanocrystals in solution [18], a) intensity plot, b) pair correlation function g.

V. Conclusion

In summary, in this paper we have examined some of the methods used in spatial statistics to characterize 2D point patterns. In particular, the breakdown spots distribution in MIS and MIM devices was thoroughly analysed. In addition, we have shown some examples from nanoscience reported in the literature. Further investigation is required to identify why the breakdown spots are sometimes visible and sometimes not, and what connection exists with the materials that the structure is comprised of. According to our observations, it is not an exclusive matter of the semiconductor substrate (Si and InP), the oxide material (MgO and HfO_2) or the gate electrode (Pt and NiSi). Other issues to be addressed that will help to increase our understanding about the formation of the point pattern are the following: Are all the breakdown events

observable or only those associated with hard breakdown? Does the spatial-temporal nature of the phenomenon play any role? What is the material of the filamentary path running across the oxide layer? We hope all these questions can be solved in the near future.

ACKNOWLEDGMENTS

E.M. acknowledges the support of the Spanish Ministry of Science and Technology under contract number TEC2009-09350 (partially funded by the European Union FEDER program) and the Departament d'Universitats, Recerca i Societat de la Informació de la Generalitat de Catalunya under contract number 2009SGR783. P.K.H. acknowledges the SFI grant ("09/IN.1/I2633 INVENT"). J.S. also acknowledges the ICREA ACADEMIA award. The authors also acknowledge D. O'Connell from Tyndall National Institute for samples processing.

REFERENCES

[1] J. Illian, A. Penttinen, H. Soyan, D. Stoyan, in *Statistical analysis and modelling of spatial point patterns*, Wiley, 2008
[2] P. Diggle, in *Statistical analysis of spatial point patterns*, Arnold, 2003
[3] M. Alam, D. Varghese, B. Kaczer, "Theory of breakdown position determination by voltage- and current-ratio methods", *IEEE Trans Elect Dev* 55, 3150 (2008)
[4] M. Alam, R. Smith, "A phenomenological theory of correlated multiple soft-breakdown events in ultra-thin gate dielectrics", *Proc. IRPS* 2003, p. 406
[5] J. Suñé, E. Wu, "Statistics of successive breakdown events in gate oxides", *IEEE Elect Dev Lett* 24, 272 (2003)
[6] E. Miranda, E. O'Connor, P.K. Hurley, "Analysis of the Breakdown Spots Spatial Distribution in Large Area MOS Structures", *Proc. IRPS* 2010, p. 775
[7] E. Wu, J. Stathis, L. Han, "Ultra-thin oxide reliability for ULSI applications", *Semicond Sci Technol* 15, 425 (2000)
[8] A. Baddeley, R. Turner, "Spatstat: An R Package for Analyzing Spatial Point Patterns", *J Stat Software* 12, 1 (2005)
[9] M. Morishita, "Measuring of the dispersion of individuals and analysis of the distributional patterns". Memoir of the Faculty of Science, Series E2, Kyushu University, 215 (1959)
[10] A. Mathai, R. Moschopoulos, G. Pederzoli, "Random points associated with rectangles", *Rendiconti del Circolo Matematica di Palermo* XLVIII, 163 (1999)
[11] H. Uchida, I. Aikawa, N. Hirashita, T. Ajioka, "Enhanced degradation of oxide breakdown in the peripheral region by metallic contamination", *Proc. IEDM* 1990, 405
[12] Y. Li, Zz. Tokei, Ph. Roussel, G. Groeseneken, K. Maex, "Layout dependency induced deviation from Poisson area scaling in BEOL dielectric reliability", *Mic Rel* 45, 1299 (2005)
[13] S. Cunningham, S. MacKinnon, "Statistical methods for visual defect metrology", *IEEE Trans Semic Manu* 11, 48 (1998)
[14] J. López De La Cruz, M. Gutiérrez, "Spatial statistics of pitting corrosion patterning: Quadrat counts and the non-homogeneous Poisson process", *Corr Sci* 50, 1441 (2008)
[15] J. Scalon, N. Fieller, E. Stillman, H. Atkinson, "Spatial pattern analysis of second-phase particles in composite materials", *Mat Sci Eng* A356, 245 (2003)
[16] http://iap.physnet.uni-hamburg.de/group_g/index.en.php
[17] http://ischuller.ucsd.edu/research/nanodots.php
[18] http://www.physorg.com/news168874003.html